Aerospace Technology Congress
11-12 October 2016, Solna, Stockholm

MODELLING AND CONTROL OF A LONG FLEXIBLE GUYED STRUCTURE

P. Kurka*, P. Gonzalez*, L. H. Teixeira* and J. Izuka**

* Faculty of Mechanical Engineering, University of Campinas, 200 Mendeleyev St, Campinas-SP, Brazil.
(E-mail: kurka@fem.unicamp.br, pagora00@fem.unicamp.br, l147099@dac.unicamp.br)
** Faculty of Applied Sciences, University of Campinas, 1300 Pedro Zaccaria St, Limeira-SP, Brazil
(E-mail: jaime.izuka@fca.unicamp.br)

ABSTRACT

The objective of this work is to determine a dynamic model to represent a long, flexible deployable structure, aiming its vibration control. We propose a modeling strategy in order to overcome the problems related to the construction of numerical parametric models of exploration probes, shaped as long deformed beams with variable cross section, subject to self-weight and concentrated loads The proposed modeling strategy consists in finding the static large deformation curve of the beam subjected to the pulling cable force. Then, a coarse finite elements mesh is adapted to the static deformed shape of the pulled beam, yielding a linear model of the dynamic parameters. The modeling strategy is also applied to characterize the static and dynamic behaviors of a real beam. The H∞ control methodology is applied to the numerical dynamic model in order to suppress the vibration of the flexible beam with large deformations. The control strategy design is based on the modal characteristics of the structure. The results show that the proposed strategy of combining an analytical model of static deformation with a low order finite element model of the solid is an efficient way to obtain a convenient dynamic description of the structure.

KEYWORDS: Flexible beams with variable cross sections, Finite Element Method, Vibration of Guyed Beams.

INTRODUCTION

The use of long, flexible deployable structures applied in space exploration vehicles in low-gravity environment applications was the motivation of this work. The advantages of such structures are their lightweight and the capability to withstand large displacements without exceeding their specified elastic limit (Puig et al. 2010, Tibert 2002 and Pellegrino 2001). Space exploration vehicles for example may benefit from the use of a long controllable beam manipulator with sensors attached to its end, to reach regions of scientific interest such as mountain slopes or the face of steep terrains. The beam´s tip end positioning can be achieved by deflecting the flexible structure through lightweight cables instead of heavy actuators, which contributes to the weight restriction. Moreover, vibration control of its free end is essential for a practical application. The use of cable or tendon as an actuator in the vibration control of flexible structures is found in the work of Nudehi (2006), who used a compressive buckling-type end load for active vibration control of a cantilever beam. Sohn (2008) used shape memory alloy (SMA) wire actuators to control the position and vibration of a flexible beam structure. The use of cable tension for active vibration control in frame structures has been investigated by Issa (2010). Vibration control of large structures, for example suspension brigdes, can also be done using active tendon theory as presented by Preumont (2008, 2015, 2016). In this context, the objective of this study is to determine a dynamic model for a long and flexible structure, aiming its vibration control.

We propose a modeling strategy in order to overcome the problems of construction of numerical parametric models of exploration probes, shaped as long deformed beams with variable cross section, subject to self-weight and concentrated loads. The first step in the proposed modeling strategy consists in finding the static deformation curve of the beam subjected to the pulling cable force. The differential equations that represents the non-linear behavior of beams subject to large deformation can be solved through elliptic integrals (Frish–Fay 1962, Timoshenko and Gere 1961, Yau 2010) or numerical approximations (Ohtsuki 2001, Shvartsman 2007, Holland et al. 2006, Howell 2001 and Al-Sadder and Al-Rawi 2006). |In this work, we choose the numerical method (shooting method) to calculate the static deformation. Then, a coarse FE mesh is adapted to the static deformed shape of the pulled beam, yielding a linear dynamic model from which we calculate the eigen modes and eigen frequencies of the structure.

Vibration control of flexible beams can be performed by different control designs. Proportional-integral-derivative (PID) controller (Khot 2013), linear quadratic Gaussian control (Ma 2015), robust vibration control (Hao 2014) and H∞ control (Zhang 2013 and Sharma 2014) are the control strategies used to attenuate vibration of such structures. In this work, the H∞ control methodology is applied to the numerical dynamic model in order to suppress the vibration of the flexible. The control strategy design is based on the modal characteristics of the structure.

This paper is presented as follows. **Methods** introduces the equation representing the elastica of the beam with large deformation and variable transversal section, subjected to the action of pulling cables. We also presents the basic 3D beam element, which was used to build the FE model that are adapted to the static deformed shape of the pulled beam. **Numerical and experimental results** describes the experimental setup, simulation and experimental results, as well as the control method used to attenuate the vibrations of the beam. **Discussion** examines the results obtained and draws the relevant conclusions.

METHODS

The structure that represents the flexible arm is simplified to a long tapered beam subject to the pulling force of the cable. We considered a geometric nonlinear situation since the flexible arm is subject to a large deformation. One difficulty is that the pulling force direction depends on the tip position, which is the problem unknown. The shooting method is applied to solve the differential equation that represents this problem. Once the flexible arm deformation is calculated, it´s vibration characteristics is obtained from a FE model meshed on the spatial coordinates of the points of the deformed structure. Such characteristics are used in the control design.

Static Deformation Model

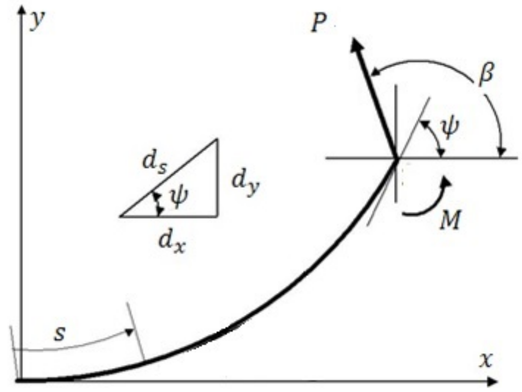

Figure 1: Beam with forces P

The bending moment is proportional to the change in curvature caused by the applied loads, according to the classical Bernoulli-Euler theory for the deflection of beams, (Frisch-Fay, 1962). Such a relation can be written as

$$\frac{M}{EI} = \frac{d\psi}{ds}. \tag{1}$$

It can be seen in the figure, also that

$$\sin\psi = \frac{dy}{ds}, \tag{2}$$

and

$$\cos\psi = \frac{dx}{ds}. \tag{3}$$

The beam is loaded with a concentrated force P, the external moment M and distributed weight w as shown in Figure 2, leading to the following equation of equilibrium of moments

$$EI\frac{d\psi}{ds} = M + P\sin\beta\ (b_x - x) - P\cos\beta_3\left(b_y - y\right) + \int_s^L w\big(x(\xi) - x(s)\big)d\xi\ , \tag{4}$$

where b_x and b_y are the horizontal and vertical projections, s is the length of a generic position in the section, β is the inclination angle of force P, ξ is a local length variable and L is the total length.

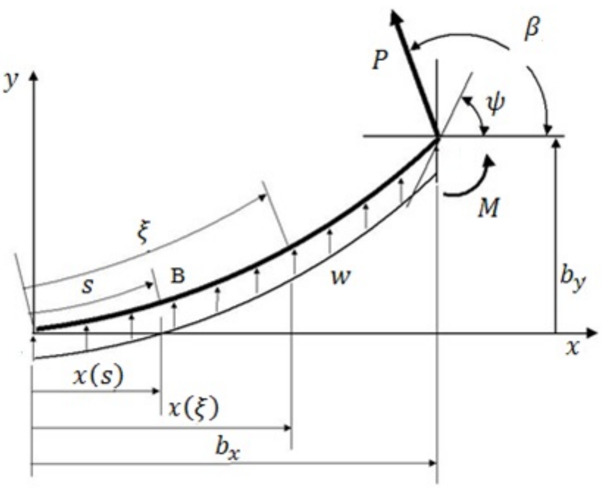

Figure 2: Characteristics of the beam and the distributed load w

The moment of inertia is defined as

$$I = \pi \frac{D(s)^4}{64}, \tag{5}$$

where D is the varying cross section diameter given by

$$D(s) = \left(1 - \left(1 - \frac{D_2}{D_1}\right)\frac{s}{L}\right) D_1. \tag{6}$$

Differentiation of the left hand side of Eq.(4) with respect to s, leads to:

$$\frac{d}{ds}\left(EI\frac{d\psi}{ds}\right) = \frac{EI}{L^2}(1 - \Delta D\, u\,)^4 \left(\frac{d^2\psi}{du^2} - \frac{4\Delta D}{(1 - \Delta D u)}\frac{d\psi}{du}\right), \tag{7}$$

where

$$\Delta D = \left(1 - \frac{D_2}{D_a}\right), \tag{8}$$

and

$$u = \frac{s}{L}. \tag{9}$$

Differentiation of the right hand side of Eq.(1) with respect to s leads to:

$$\frac{d}{ds}\left(M + P\sin\beta\ (b_x - x) - P\cos\beta\left(b_y - y\right) + \int_s^L w\big(x(\xi) - x(s)\big)d\xi\right) = \Gamma_1 + \Gamma_2, \tag{10}$$

where

$$\Gamma_1 = \ -P\sin(\beta - \psi), \tag{11}$$

and

$$\Gamma_2 = -\frac{\rho\pi g L}{12}\{D_1^2 + D_1 D_2 + D_2^2 - 3D_1^2 u + 3(D_1^2 - D_1 D_2)u^2 - (D_1^2 - 2D_1 D_2 + D_2^2)u^3\}. \tag{12}$$

The equilibrium equation of moments can be finally written by equaling Eq. (7) and (10) as

$$\frac{d^2\psi}{du^2} - \frac{4\Delta D}{(1-\Delta D u)}\frac{d\psi}{du} = \frac{L^2}{EI(1-\Delta D\, u)^4}(\Gamma_1 + \Gamma_2)\,. \tag{13}$$

The boundary conditions are

$$\psi_{u=0} = 0\,, \tag{14}$$

and

$$\left(\frac{d\psi}{du}\right)_{u=1} = \frac{d\psi_2}{ds} = \frac{L}{EI_2}M. \tag{15}$$

The presented method was applied to find the deformed shape of the structure when subject to a pulling force of a cable. Based on this geometry, a FE model was meshed in order to find the stiffness and mass matrix of the beam and cable. In the next section, the FE model is presented.

Finite Elements Model

The theoretical vibration characteristics of the structure were obtained numerically, based on the FE model of the structure. 3D beam elements with axial, bending and torsional stiffness are employed to represent the mesh the FE model. The pulling cable is represented by linear spring elements. The 3D beam elementary stiffness and mass matrix are obtained using the Galerkin formulation for the weighted residuals method (Bathe 1996).

In order to find a truss element stiffness and mass matrix, we apply Newton's second law to the truss element and considering it's weak formulation, we have

$$I = \int_0^L \left(\rho A\frac{\partial^2 u}{\partial t^2} + \frac{\partial}{\partial x}\left(AE\frac{\partial u}{\partial x}\right)\right)\omega dx\,, \tag{16}$$

where ρ is density, A is section area, L is the element length, ω is the test function or shape function, u is the axial coordinate along x axis and t is time.

For beam elements, we consider the Euler Bernoulli equation for beam bending. The average weight residual of this equation is

$$I = \int_0^L \left(\rho\frac{\partial^2 v}{\partial t^2} + \frac{\partial^2}{\partial x^2}\left(EI\frac{\partial^2 v}{\partial x^2}\right)\right)\omega dx\,, \tag{17}$$

where v is the transverse displacement of the beam, I is the moment of inertia and E is the Young Modulus.

The torsion behavior can be computed from Saint Venant torsion problem. Considering it's weak form, we have

$$I = \int_0^L \left(\rho J \frac{\partial^2 \theta}{\partial t^2} + \frac{\partial}{\partial x}\left(GJ \frac{\partial \theta}{\partial x} \right) \right) \omega dx \,, \tag{18}$$

where θ is the torsion angle along axial direction, G is the shear modulus and J is the polar second moment of area.

Considering a linear shape function for truss (Equation (19)) and torsion (Equation(20)) element, third order polynomial for beam (Equation (21)) element and by integrating the matrix terms, we can calculate the element stiffness and mass matrices.

$$u = \omega_1 u_1 + \omega_2 u_2 \tag{19}$$

where $\omega_1 = \frac{L-x}{L}$ and $\omega_2 = \frac{x}{L}$.

$$v = \omega_1 v_1 + \omega_2 \theta_1 + \omega_3 v_2 + \omega_4 \theta_2 \tag{20}$$

Where $\omega_1 = 1 - \frac{3x^2}{L^2} + \frac{2x^3}{L^3}$, $\omega_2 = x - \frac{2x^2}{L} + \frac{x^3}{L^2}$, $\omega_3 = \frac{3x^2}{L^2} - \frac{2x^3}{L^3}$ and $\omega_4 = -\frac{x^2}{L} + \frac{x^3}{L^2}$

$$\theta = \omega_1 u_1 + \omega_2 u_2 \tag{21}$$

where $\omega_1 = \frac{L-x}{L}$ and $\omega_2 = \frac{x}{L}$.

The 3D beam element can be obtained from the combination of the presented axial, bending and torsional stiffness and corresponding inertial behavior. Such element presents 12 degrees of freedom (DOF) as described in Eq. 22 and Figure 3.

$$\boldsymbol{r}_e^T = [r_1 \quad q_1 \quad o_1 \quad \theta_{x1} \quad \theta_{y1} \quad \theta_{z1} \quad r_2 \quad q_2 \quad o_2 \quad \theta_{x2} \quad \theta_{y2} \quad \theta_{z2}]. \tag{22}$$

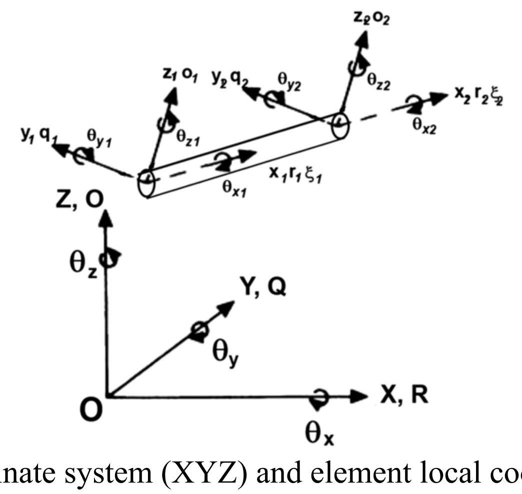

Figure 3: Global coordinate system (XYZ) and element local coordinate system (RQO).

The local coordinates vector $\boldsymbol{r}_e$, shown in Figure 3, can be transformed into a global coordinate system $\boldsymbol{R}_e$ with the relation

$$\boldsymbol{R}_e = \mathbf{T}^{\mathrm{T}}\ \boldsymbol{r}_e \tag{23}$$

where $\mathbf{T}$ is the transformation matrix with the angles formed between the local and global coordinates. The stiffness and mass matrices are described respectively as

$$\mathbf{K_e} = \mathbf{T^T}\bar{\mathbf{k}}_\mathbf{e}\mathbf{T}, \tag{24}$$

$$\mathbf{M_e} = \mathbf{T^T}\bar{\mathbf{m}}_\mathbf{e}\mathbf{T}. \tag{25}$$

The linear beam element mass and stiffness matrices are defined in the element coordinate system. In order to represent this element in the global coordinate system, a transformation matrix **T** is used which converts the element's coordinates to the global coordinates system. Matrix **T** is defined, based on the position of the element nodes in the global coordinate system. The finite element model of the long probe is modeled with 10 beam elements with 12 DOF and the cable is modeled as truss element with 2 DOF. The cable stiffness is representative only for axial direction.

NUMERICAL AND EXPERIMENTAL RESULTS

The prototype required to validate this methodology should withstand large deformation, while its material properties must respond in the linear field. For this purpose, a cantilever fiberglass fishing rod is used in order to compare its static large deflection and dynamics characteristics to the simplified numerical model. The beam is deformed by the action of a tip end pulling cable and a hanging mass, as shown in Figure 4. The physical characteristics of the fiberglass beam are presented in Table 1.

Table 1 - Test beam characteristics

Length	Cross section diameter 1	Cross section diameter 3	Modulus of elasticity	Density
0.965 (m)	0.0081 (m)	0.0015 (m)	35 (GPa)	2150 $\left({}^{\mathrm{kg}}/_{\mathrm{m}^3}\right)$

Static Deformations

Experimental tests are carried out to validate the static modeling procedure described in section **Static Deformation Model**. The vertical and horizontal deflections of selected points on the beam, as shown in Figure 4, were measured with the support of an altimeter, a set-square and a base.

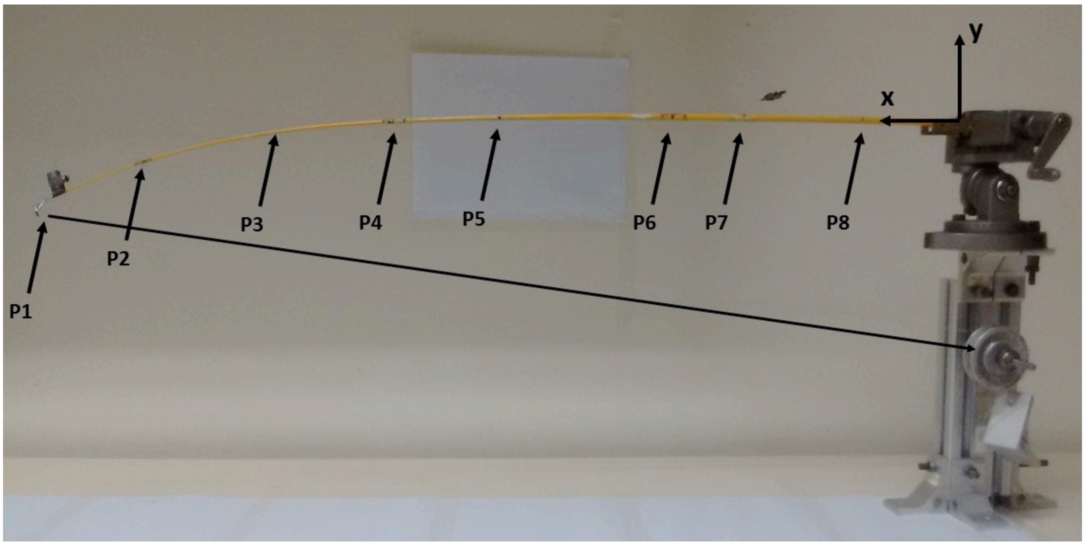

Figure 4: Configuration for the static deflection measurements

The deformed beam configurations are obtained from the pull of a nylon cable attached to the free end of the beam. Moreover, the cable is tensioned with the support of five different weights and a pulley as shown in Figure 4. The cable origin coordinates are 0.040m (horizontal) and -0.233m (vertical) and its stiffness is 1 kN/m. The angle of the traction force is defined by the positions of the tip end and cable clamp. A 15 grams accelerometer used to obtain the experimental vibration data, works also as an end hanging load as seen in Figure 5.

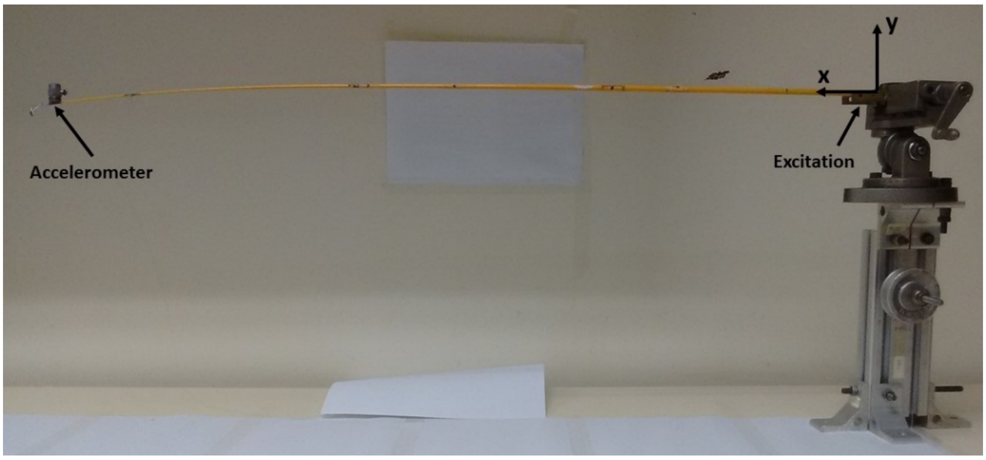

Figure 5: Beam for vibration test with the position used to excite the structure.

The measurements were performed to six different configurations due to six distinct weights, as shown in Figure 6. Then, deflections obtained from the experimental analysis and the theoretical model were compared, as seen in Figure 7. Results show good agreement between experimental measurements and numerical results.

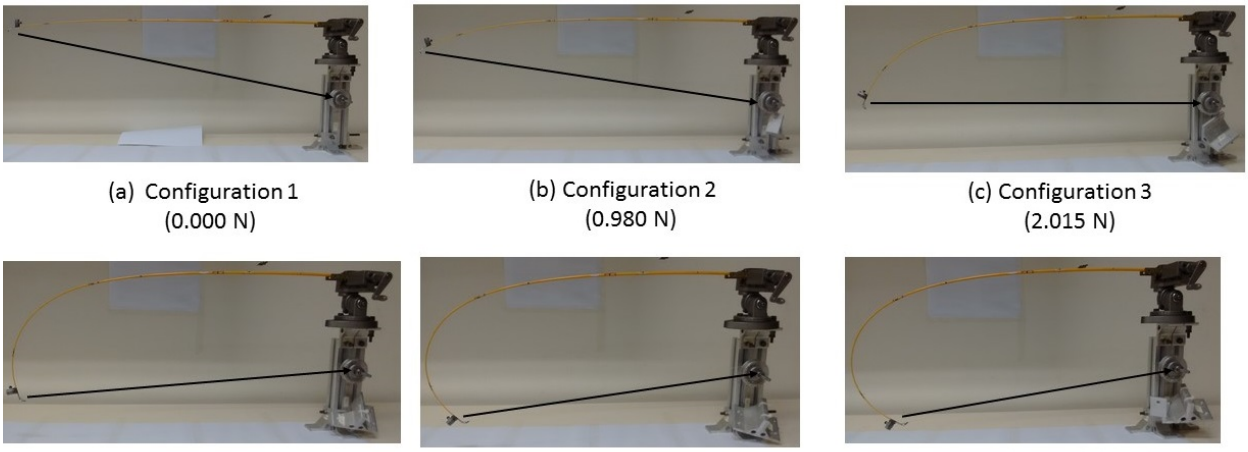

(a) Configuration 1 (0.000 N)
(b) Configuration 2 (0.980 N)
(c) Configuration 3 (2.015 N)
(d) Configuration 4 (2.995 N)
(e) Configuration 5 (4.020 N)
(f) Configuration 6 (5.000 N)

Figure 6: Configurations of the beam for different pulling cable tractions.

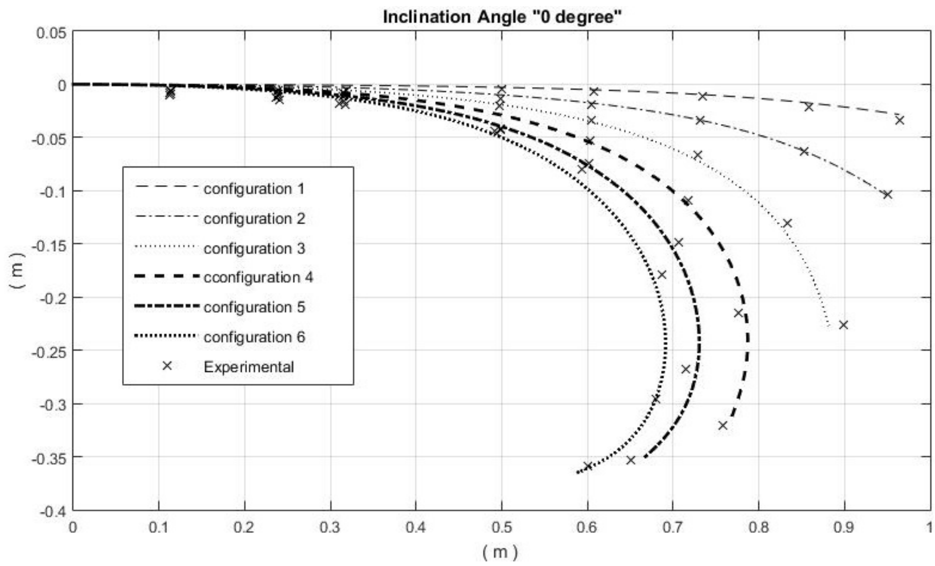

Figure 7: Comparison between numerical and experimental static results.

Dynamic characteristics

Modal analysis techniques were used to validate the dynamic model of the beam described in section **Finite Element Model**. The structure's natural frequencies were obtained by analyzing the frequency response of the system due to an impulse input applied by an impact hammer. Moreover, the same modal characteristics are calculated numerically from the mass and stiffness matrices of the proposed theoretical model.

The signal sent by the accelerometer is sampled and processed with the support of a Photon+ dynamic signal analyzer and the software RT Pro Photon®. The six beam deformed configurations described at section **Static Deformations** (Figure 6) were tested.

Vibration results are also calculated using the finite element model generated for each static deformed configuration shown in Figure 6. The theoretical natural frequencies are compared with experimentally measured results. Table 2 shows the first ten modes calculated from the finite element model. Configurations 1 to 6 (Config1 to Config6 of the Figure 6) correspond to the different pulling load conditions.

Table 2 - Natural Frequency calculated theoretically by the finite element method

Modes	Config1 (Hz)	Config2 (Hz)	Config3 (Hz)	Config4 (Hz)	Config5 (Hz)	Config6 (Hz)
1	4.40	4.42	4.52	4.74	4.97	5.14
2	4.40*	5.76*	6.52*	6.87*	7.19*	7.44*
3	16.18*	16.08	15.41	14.48	13.85	13.49
4	16.21	23.99*	28.80*	28.67*	27.83*	26.91*
5	42.14*	41.90	40.08	37.71	36.06	35.01
6	42.22	46.38*	58.91*	63.75*	64.38*	63.28*
7	82.17*	81.87*	79.35	75.07*	70.84*	68.56*
8	82.29	81.87	79.41*	75.69	72.82	71.04
9	136.42*	134.78*	128.15*	122.02*	118.25*	116.60*
10	136.53	136.07	133.17	128.71	125.24	123.26

* Vibration modes in the XY plane.

Table 3 - Natural Frequency obtained experimentally

Modes	Config1 (Hz)	Config2 (Hz)	Config3 (Hz)	Config4 (Hz)	Config5 (Hz)	Config6 (Hz)
1	3.30	2.81	2.81	3.28	3.28	4.06
2	(i)	6.04	5.68	5.49	6.23	6.41
3	16.11	12.97	14.28	13.92	15.20	14.80
4	(ii)	19.59	23.80	25.82	28.02	28.21
5	44.68	41.38	40.01	37.35	41.56	41.38
6	(iii)	47.61	53.10	54.11	61.34	61.34
7	76.17	91.19	86.43	71.50	74.16	71.41
8	(iv)	(iv)	(iv)	(iv)	(iv)	(iv)
9	112.80	120.80	119.92	119.81	115.50	111.30
10	(v)	(v)	(v)	(v)	125.80	124.40

(i) The first and second vibration modes are very close.
(ii) Third and fourth vibration modes are very close.
(iii) The sixth and fifth vibration modes are very close.
(iv) The seventh and eighth vibration modes are very close.
(v) The ninth and tenth vibration modes are very close.

Configuration 1 (traction force of 0.0 N), presents two orthogonal vibration modes in plane XY and XZ with similar natural frequencies. This can be observed in both theoretical and practical calculations shown in Tables 2 and 3, respectively. This behavior is caused by the symmetrical geometry of the circular section of the beam.

Configuration 2 (traction force of 0.980 N) brings a change in the pattern of natural vibration modes. Modes 1, 2, 3, 4, 5 and 6 have all distinctive natural frequencies. Modes 1, 3 and 5, represent an oscillation in the XZ plane, with greater amplitude on the Z axis. Modes 2, 4 and 6 display a greater oscillation on the Y axis. Such a behavior can be observed in the experimental data of

Table 3. The remaining modes retain similar patterns as observed in configuration 1, where two modes have close vibration frequencies in orthogonal planes. The experimental data confirms the predicted values of such frequencies.

Configurations 3 to 6 (traction force of 2.015 N to 5.000 N) are similar to configuration 2 with respect to the modes and frequencies of vibration 1, 2, 3, 4, 5 and 6. As the traction force of the cable increases, modes 7 and 8, 9 and 10 display different frequencies. The experimental results of configuration 3 and 4 did not verify such a behavior due to the small difference in frequency values. It was possible to observe in configuration 5 and 6, the difference of frequencies between modes 9 and 10.

The vibration frequencies obtained by the impact hammer test show good agreement with the theoretical results of the numerical model. The validated numerical model is used in a numerical simulation control of a flexible structure vibration, shown in the next section.

VIBRATION CONTROL

The vibration control of the flexible structure is presented in this section. The design of an H∞ controller is shown and theoretical and experimental results are then compared.

Design of the controller

An H∞ controller is designed to suppress the vibration of the structure. The controlled system scheme is shown in Figure 8, where d is the input vector with the disturbance force and n is the measurement noise.

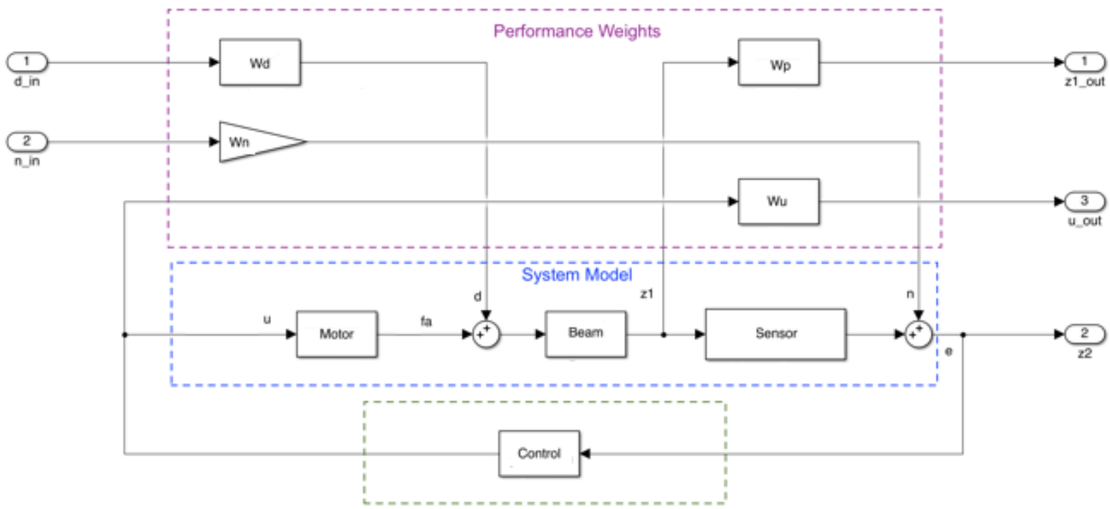

Figure 8: Block Diagram

System model

The mathematic model of the general system is

$$\dot{\boldsymbol{v}}(\mathbf{t}) = \mathbf{A}\boldsymbol{v}(\mathbf{t}) + \mathbf{B}_w \boldsymbol{w}(\mathbf{t}) + \mathbf{B}_u \mathrm{u}(t), \qquad (26)$$
$$\mathbf{z}(\mathbf{t}) = \mathbf{C_1}\boldsymbol{v}(\mathbf{t}) + \mathbf{D}_{1w}\boldsymbol{w}(\mathbf{t}) + \boldsymbol{D}_{1u}\mathrm{u}(t),$$

$$\boldsymbol{e}(\mathbf{t}) = \boldsymbol{C_2}\boldsymbol{v}(\mathbf{t}) + \boldsymbol{D}_{2w}\boldsymbol{w}(\mathbf{t}) + D_{2u}\mathrm{u}(t).$$

where, $\boldsymbol{v}(\mathbf{t})$ is the state vector, $\boldsymbol{w}(\mathbf{t})$ is an input vector with the disturbance force, the control signal is represented by $\mathrm{u}(t)$, input control vector by $\boldsymbol{e}(\mathbf{t})$ and $\mathbf{z}(\mathbf{t})$ is the performance vector that represents the system response signals to be controlled. $\mathbf{A}$ is comprised from the motor and beam dynamic matrices. $\mathbf{B}_w$ and $\mathbf{B}_u$ are input matrices $\mathbf{C_2}$, $\mathbf{D}_{2\mathrm{w}}$ and D_{2u} are output matrices. Matrices $\mathbf{C_1}$, $\mathbf{D}_{1w}$ and $\boldsymbol{D}_{1u}$, are chosen to define the desired performance goals.

An AC servo motor and a MINAS 4S driver, configured in torque control mode, is used to pull the driving cable. The motor´s model is obtained experimentally using MATLAB's identification tool and a data acquisition board.

The pulling force actuator is defined by the torque of the servomotor and the radius of a pulley placed in the motor's shaft. In practice, the motor has a dead zone. Such a nonlinearity is modeled in Simulink diagram blocks, and also used in the design of the controller.

The vibration of the tip of the beam is measured by means of a custom built infrared spring displacement sensor, fitted in line with the pulling cable. The sensor's elastic characteristic is included in FE model of the beam and cable. A polynomial expression is experimentally built to express the direct relation between force - F_s (N) and voltage - v_s (V), measured in the optical displacement sensor.

The dynamic FE model of the beam has the form

$$\begin{bmatrix} \dot{\boldsymbol{x}}_1 \\ \dot{\boldsymbol{x}}_2 \end{bmatrix} = \begin{bmatrix} \mathbf{0} & \mathbf{I} \\ -\mathbf{M}^{-1}\mathbf{K} & -\mathbf{M}^{-1}\mathbf{D} \end{bmatrix} \begin{bmatrix} \boldsymbol{x}_1 \\ \boldsymbol{x}_2 \end{bmatrix} + \begin{bmatrix} \mathbf{0} \\ -\mathbf{M}^{-1}\boldsymbol{b}_w \end{bmatrix} \boldsymbol{w}(\mathbf{t}) + \begin{bmatrix} \mathbf{0} \\ -\mathbf{M}^{-1}\boldsymbol{b}_{fa} \end{bmatrix} \mathrm{f_a}(\mathrm{t})$$
$$\boldsymbol{y}(\boldsymbol{t}) = [\mathbf{1} \quad \mathbf{0}] \begin{bmatrix} \boldsymbol{x}_1 \\ \boldsymbol{x}_2 \end{bmatrix}, \tag{27}$$

where $\boldsymbol{x}$ is the state vector, $\mathbf{M}$ is the mass matrix, $\mathbf{D}$ is the damping matrix, $\mathbf{K}$ is the stiffness matrix. $\boldsymbol{b}_w$ and $\boldsymbol{b}_{f_a}$ are $\mathrm{n} \times 1$ vectors, comprised of elements either 0 or 1, depending on the position of the disturbance input and on the position of the control force input, respectively. $\boldsymbol{w}(\mathbf{t})$ is the disturbance force acting on the beam and $\mathrm{f_a}(\mathrm{t})$ is the force of the cable pulled by the actuator. Tip displacement $\boldsymbol{y}(\boldsymbol{t})$ is the output signal.

The damping matrix $\mathbf{D}$ is defined as proportional to stiffness and mass matrix

$$\mathbf{D} = \sigma\mathbf{M} + \tau\mathbf{K}, \tag{28}$$

where $\sigma = 1\times10^{-5}$and $\tau = 1\times10^{-3}$.

Control Design

Schur method is used to calculate the controller gain, based on the state space description of the reduced order model of the system. The model is truncated in the first two modes, which correspond to the lowest frequencies. Weighting functions are used to emphasize the frequency range where the controller must actuate. Low pass and high pass filters are used as weighting functions. In the present work, *Wu* represents the equations of a high pass filter which emphasizes the high frequency region of the control effort signal. *Wp* and *Wd* represents the equations of low pass filters which emphasize the low frequency region of the performance signals of system output and disturbance. Figure 9 shows the frequency response characteristics of the system and filters. The two lowest frequencies, 36.2rad/s and 152rad/s, are used to design the controller.

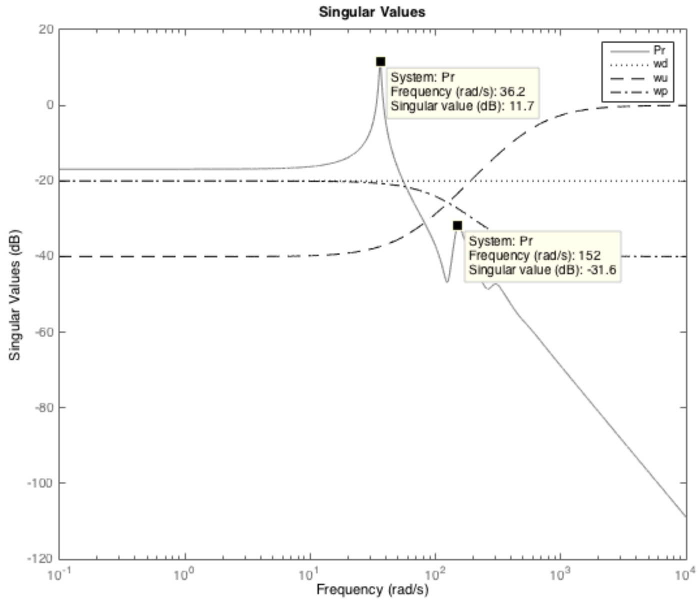

Figure 9: Set of the weight functions.

The subroutine *hinfsyn* of MATLAB is used, together with the complete model, to calculate the robust controller from the connection of the weight functions.

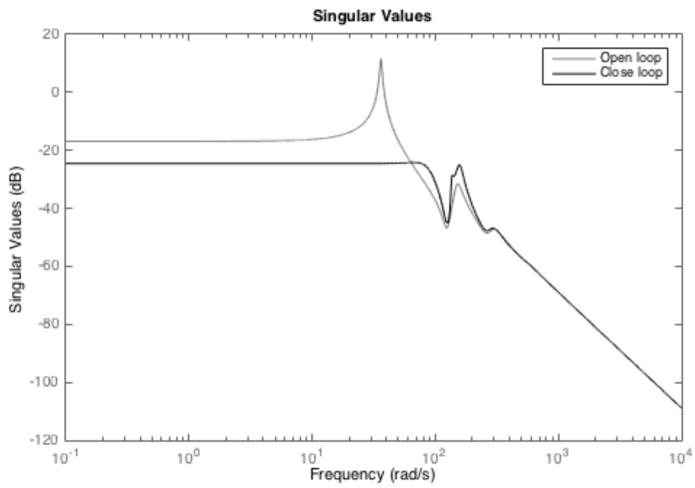

Figure 10: Frequency response of the system with uncontrolled and controlled vibration.

The single values of all system model in open loop and closed loop are presented in Figure 10. The Robust control can reduce the highest peak of the frequency selected in the reduced model. It is possible to see that the frequencies that were not part of the control strategy are still present.

The infinite norm of the system without control is 3.8326, while with the action of the control, it is minimized to 0.0613.

The control strategy is validated by numerical simulations. The transient response of the system in open loop (uncontrolled) and closed loop are shown in Figure 11. Simulation results show that the closed loop control attenuates the vibration of the free end of the beam in less than 0.5s, as opposed to the uncontrolled movement that lasts beyond the remaining 5 seconds of the time response observation window.

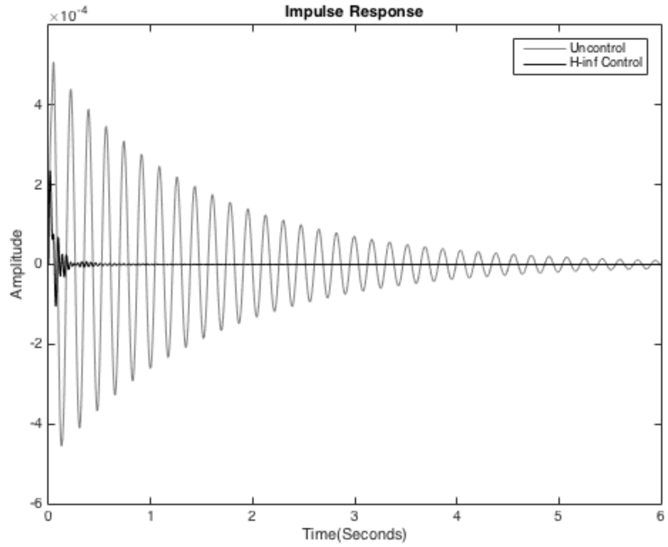

Figure 11: Impulse response in open and closed loop

In the second simulation, the beam's end is subjected to simultaneous random vibration of 1 N RMS values in X and Y directions. The resulting vibration response of the beam's tip without control (grey line) and with control actuation (black line) are shown in Figure 12. In this case, the vibration levels are reduced to about 20% of the intensity of uncontrolled vibrations.

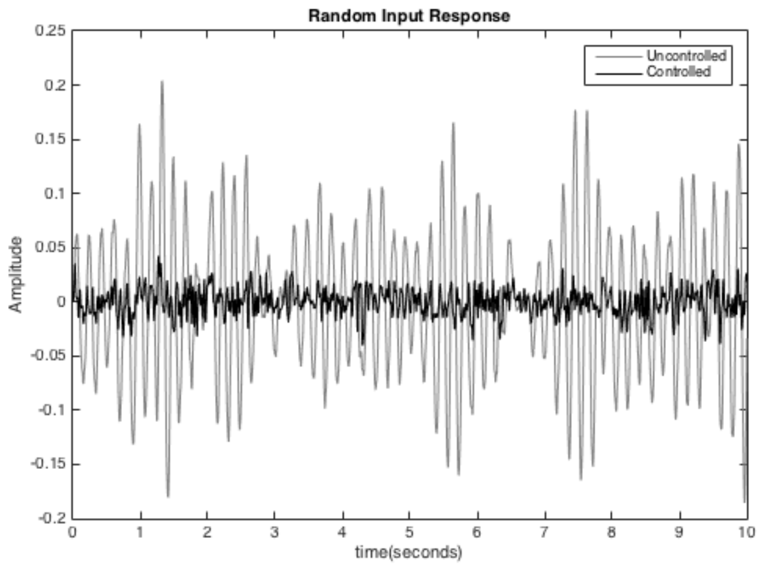

Figure 12: System response with uncontrolled and controlled vibration due to a random input on the tip of the beam

The control strategy is validated by a practice test. The next section shows the results of system vibration attenuation to a flexible beam with large deformations.

Experimental results of the vibration control design

In the practical test, a cantilever fiberglass fishing rod is used with the following dimensions: length of 1.185m and cross section diameter varying from $8{,}8\ 10^{-3}m$ to $2{,}0\ 10^{-3}m$. The material properties are: Young modulus of 4.4GPa and mass density of $2.000\ ^{\mathrm{kg}}/_{\mathrm{m}^3}$. The fishing rod's free end is pulled by a flexible copper cable attached to a pulley connected to an AC servo motor. A MINAS 4S driver is used in a torque control mode in order to drive the motor. The motor pulls and releases the tensioned cable to control the movement of the free end of the beam, which is measured by an infrared deformation sensor. MATLAB's Simulink platform is used to send the control signal through a NATIONAL INSTRUMENTS PCI-6229 analog input/output board. The analog input of the data acquisition board receives the output signal from the displacement sensor. The displacement signal is filtered, yielding the error signal, which is used to calculate the control signal. An illustrative scheme of the experimental setup is shown in Figure 13

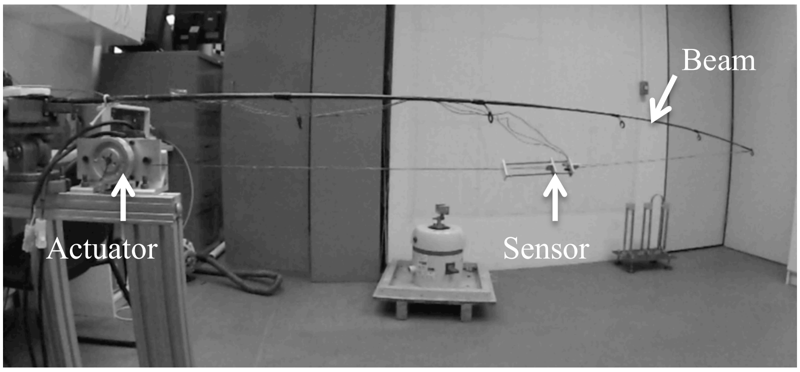

Figure 13: Experimental setup for the vibration control of a flexible beam.

The experiment consist of applying an external disturbance force at the free end of the beam, which is deformed in a specific configuration. The transient response of the system in open loop (uncontrolled) situation is shown in Figure 14a. The transient response of the system in closed control loop is seen in Figure 14b. The practical experiment shows that the closed loop control attenuates the vibration of the free end of the beam in about 1s, as opposed to the uncontrolled movement that lasts for more than 4 seconds. Due to different physical and electrical sources, we can notice a considerable noise affecting the experimental signals, which makes the control actuation less evident when compared to the numerical simulation showed in Figure 11.

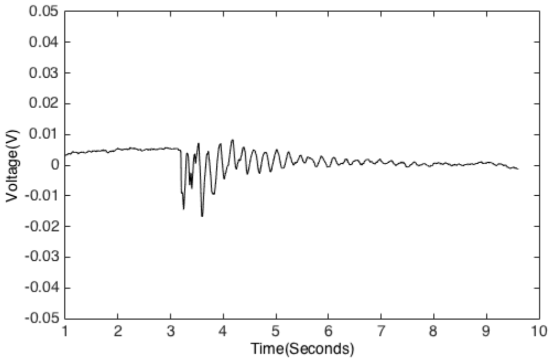

Figure 14a.: Sensor output signal in open loop

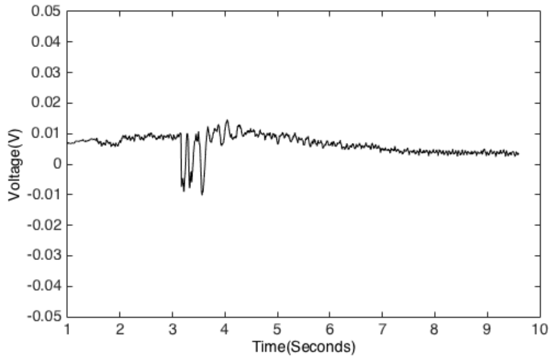

Figure 14b.: Sensor output signal in closed loop

Figure 14: Experimental results to an impulse input.

CONCLUSIONS

This work consisted in modeling a long, lightweight and flexible beam with variable cross section, pulled by a cable attached to its tip and base. The model considers also self-weight and concentrated loads. The model was verified in static and dynamic experiments. The static analytical and experimental deformations of a long beam were verified, for five different loads. The comparison between theoretical and practice calculations shown a good approximation between the two results, as shown in Figure 7. Moreover, in a dynamic experiment, the beam was deformed by action of a pulling cable, under six different loading configurations as shown in Table 2 and Table 3.

The results indicate that the proposed strategy of combining an analytical model of static deformation with a low order finite element model of the solid is an efficient way to obtain a convenient dynamic description of the structure. Results from numerical simulation and practice of the vibration control, through an $H\infty$ algorithm show a considerable reduction of the beam's tip vibration, when compared to the uncontrolled model.

REFERENCES

Al-Sadder, S. and Al-Rawi, R. 2006 Finite Difference Scheme for Large-Deflection Analysis of Non-Prismatic Cantilever Beams Subjected to Different Types of Continuous and Discontinuous Loadings. *Applied Mechanics*. **75, Nos. 8–9**, 459–473.

Bathe, K.J. 1996 *Finite Element Procedures*. Prentice Hall. New Jersey

Frisch-Fay, R. 1962 *Flexible Bars*. Butterworths, London.

Hao, Y., Duan, Z., Huang, D. 2014 Robust Vibration Control of Uncertain Flexible Structures Based on Model Reduction. *Proceedings of the 33rd Chinese Control Conference-Nanjing*. 4240-4245.

Holland, D., Stanciulescu, I., Virgin, L., and Plaut, R. 2006 Vibration and Large Deflection of Cantilevered Elastica Compressed by Angled Cable. *AIAA Journal*. **44, No. 7**, 1468–1476.

Howell, L. L. 2001 *Compliant Mechanisms*. Wiley, New York.

Issa, J., Mukherjee, R., Shaw, S. W. 2010 Vibration Suppression in Structures Using Cable Actuators. *Journal of Vibration and Acoustics*. **132, no. 031006**, 1-8.

Khot, S. M., Yelve, N., Shaik, S. 2013 Experimental Study of Active Vibration Control of a Cantilever Beam. *6th International Conference on Emerging Trends in Engineering and Technology*. 1-6.

Ma, C., Zhang, X., Xie, S., Lu, Y. 2015 Active linear quadratic Gaussian control of the vibration of a flexible beam with a time-varying mass. *Journal of Systems and Control Engineering*. 1-10.

Nudehi, S., Mukherjee, R., Shaw, S. W. 2006 Active Vibration Control of a Flexible Beam Using a Buckling-Type End Force. *Journal of Dynamic Systems, Measurement and Control*. **128**, 278-286,.

Ohtsuki, A. 2001 Analysis of the Characteristics of Fishing Rods Based on the Large-Deformation Theory. *Materials and Science in Sports, edited by Sam, F.H., Minerals, Metals and Materials Society*. 161–170.

Pellegrino, S. 2001 *Deployable Structures*. Springer, Milan.

Preumont, A., Voltan, M., Sangiovanni, A., Mokrani, B. , Alaluf, D. 2015 *Active Tendon Control of Suspension Bridges*. 1-22.

Puig, L., Barton, A., and Rando, N. 2010 A Review on Large Deployable Structures for Astrophysics Missions. *Acta Astronautica* .**67**, 12–26.

Sharma, N., Kern, D. K., Seemann, W. 2014 Vibration analysis and robust control of highly deformable beams in a heavy pinched loop configuration. *Zeitschrift fur angewandte Mathematik und Physik ZAMP*. 1-14.

Shvartsman, B. 2007 Large Deflections of a Cantilever Beam Subjected to a Follower Force. *Journal of Sound and Vibration*. **304, Nos. 3–5**, 969–973.

Sohn, J. W., Han, Y.M., Choi , S. B., Lee , Y. S., Han , M. S. 2008 Vibration and Position Tracking Control of a Flexible Beam Using SMA Wire Actuators. *Journal of Vibration and Control*. **15 no. 2**, 263–281.

Tibert, G. 2002 *Deployable Tensegrity Structures for Space Applications*. Royal Inst. of Technology, Stockholm.

Timoshenko, S., and Gere, J., 1961 *Theory of Elastic Stability*. McGraw–Hill, New York.

Yau, J. 2010 Close-Form Solutions of Large Deflections for a Guyed Cantilever Column Pulled by an Inclinations Cable. *Journal of Marine Science and Technology*. **18 No 1**, 130–136.

Zhang, K., Scorletti, G., Ichchou, M., Mieyevi, F. 2013 Phase and gain control policies for robust active vibration control of flexible structures. *Smart Materials and Structures*. **22**, 1-15.